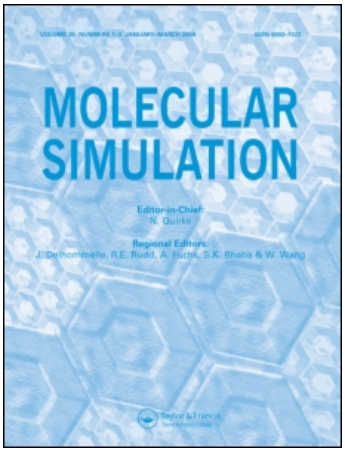

Molecular Simulation
Publication details, including instructions for authors and subscription information:
http://www.informaworld.com/smpp/title~content=t713644482

Electroosmotic Flow in Nanoscale Parallel-plate Channels: Molecular Simulation Study and Comparison with Classical Poisson-Boltzmann Theory

S. T. Cui[a]; H. D. Cochran[b]
[a] Chemical Sciences Division, Oak Ridge National Laboratory, Oak Ridge, TN, USA [b] Department of Chemical Engineering, University of Tennessee, Knoxville, TN, USA

To cite this Article Cui, S. T. and Cochran, H. D.(2004) 'Electroosmotic Flow in Nanoscale Parallel-plate Channels: Molecular Simulation Study and Comparison with Classical Poisson-Boltzmann Theory', Molecular Simulation, 30: 5, 259 — 266
To link to this Article: DOI: 10.1080/08927020410001659367
URL: http://dx.doi.org/10.1080/08927020410001659367

Molecular Simulation, Vol. 30 (5), 30 April 2004, pp. 259–266

Taylor & Francis
Taylor & Francis Group

Electroosmotic Flow in Nanoscale Parallel-plate Channels: Molecular Simulation Study and Comparison with Classical Poisson–Boltzmann Theory

S.T. CUI[a,b,*] and H.D. COCHRAN[b,a]

[a]*Department of Chemical Engineering, University of Tennessee, Knoxville, TN 37996-2200, USA;* [b]*Chemical Sciences Division, Oak Ridge National Laboratory, Oak Ridge, TN 37831-6181, USA*

(Received June 2003; In final form November 2003)

Molecular dynamics simulations have been carried out for simple electrolyte systems to study the electrokinetically driven osmotic flow in parallel-plate channels of widths ~10–120 nm. The results are compared with the classical theory predictions based on the solution to the Poisson–Boltzmann equation. We find that despite some of the limitations in the Poisson–Boltzmann equation, such as assumption of the Boltzmann distribution for the ions, the classical theory captures the general trend of the variations of the osmotic flow with channel width, as characterized by the mobility of the fluid in channels between ~10 and 120 nm at moderate to low ion concentration. At moderate concentration (corresponding to relatively low surface potential), the classical theory is almost quantitative. The theory and simulation show more disagreement at low concentration, primarily caused by the high surface potential where the assumption of Boltzmann distribution becomes inaccurate. We discuss the limitations of the Poisson–Boltzmann equation as applied to the nanoscale channels.

Keywords: Electroosmotic flow; Parallel-plate channels; Molecular dynamics simulations; Poisson–Boltzmann theory

INTRODUCTION

Fluid transport through pores and channels is widely encountered in nature and in fabricated devices. In microfluidic devices, for example, sample transport and delivery through the micrometer scale channels are precisely controlled for chemical separation and analysis [1–3]. Recently, there has been an increasing interest in fabricating and operating fluidic devices with channel dimensions of 100 nm and less. These devices with nanoscale components have potential for significantly better performance and possible novel applications in, for example, chemical separation and analysis, medical diagnosis, and drug discovery.

In fluidic devices, a widely used method for fluid transport is to drive the flow of electrolyte buffer solution electrokinetically [4]. The electric charges near the surface in the channel are driven by an electric field and carry the buffer fluid along through viscous force. Theoretical predictions on fluid transport in capillaries or parallel-plate channels have traditionally been based on the solution to the Poisson–Boltzmann (PB) equation as applied to various specific fluids and boundary conditions. The PB equation gives reasonably good predictions, provided that the ζ-potential is not too high and the ion concentration is moderate. Good accuracy is obtained also because, in most situations, the thickness of the electric double-layer is relatively small compared to the width of the microscale channels, so that the effect of the electric double-layer overlap can be disregarded. As the channel dimension decreases to nanometer scale, the effect of the electrical double-layer becomes more significant, especially when the ζ-potential is high, resulting in significant deviation of ion distribution near the wall from the assumed Boltzmann distribution, leading to a more significant effect on fluid transport in the channel.

The objectives of this study are to describe the flow in nanoscale channels in the size range between

*Corresponding author. Address: Department of Chemical Engineering, University of Tennessee, Knoxville, TN 37996-2200, USA. E-mail: scui@utk.edu

ISSN 0892-7022 print/ISSN 1029-0435 online © 2004 Taylor & Francis Ltd
DOI: 10.1080/08927020410001659367

a few tens to a few hundred nanometers and to explore the applicability of classical PB theory at such scale. The classical PB theory has been widely used in the design and analysis of experiments involving flows at micrometer scale and larger. If the classical description is applicable in nanoscale flow phenomena, it would provide great convenience in nanofluidic experiments. For this goal, we have carried out molecular dynamics simulation on simple electrolyte systems in parallel-plate channels of width from 10 to 200 nm. Because of the size range involved in such systems, it is impossible to simulate the systems using a fully atomistic description of all the solvent. As in many studies in literature, we have chosen to treat the solvent as a continuum, only the ions are explicitly modeled. Thus, the same accuracy is used for treating the solvent as in the theory. By using an explicit model for the ions, we do not make any *a priori* assumption about the ion distribution, the weak point of the theory.

Using this system, we carried out calculations to determine the ion distributions inside channels of various widths. From the ion distributions, we numerically integrated the Navier–Stokes equation to obtain the velocity profiles and the mobility of the fluid under external electric field. We analyzed the results by comparing the simulation and the classical theory as formulated by Levine *et al.* [5] for the parallel-plate channel geometry. The analysis revealed the inadequacy of the Boltzmann distribution at large surface potential. This is discussed in light of the recent experiment of Alarie *et al.* [6].

MODELS AND METHODS

In the usual Debye-Hückel theory [7], the Boltzmann distribution is approximated by the linearization of the exponentials. In the theory of Levine *et al.* [5], the Poisson–Boltzmann equation was solved using a series expansion without linearization, thus removing the errors caused by the linearization.

We briefly summarize here the classical theory describing electroosmotic flow in narrow channels. For the parallel-plate geometry, the problem becomes one of solving the one-dimensional Poisson–Boltzmann equation with appropriate boundary conditions

$$\frac{\mathrm{d}^2\psi(z)}{\mathrm{d}z^2} = -\frac{4\pi}{\varepsilon}\rho(z), \qquad \psi(0) = \psi(d) = \zeta,\ \left.\frac{\mathrm{d}\psi(z)}{\mathrm{d}z}\right|_{z=d/2} = 0, \tag{1}$$

where $\psi(z)$ is the electrostatic potential inside the fluid region between the walls, which depends on the position z in the direction normal to the walls; d is width of the channel; and ε is the dielectric constant of the fluid. The boundary conditions are the fixed potential value, ζ, at the walls ($z = 0$ and d) and the first derivative of the electrostatic potential equal to zero at the midplane in the channel ($z = d/2$). $\rho(z)$ is the electric charge density, given by the Boltzmannn distribution

$$\rho(z) = e\,n_0\left\{\exp\left(-\frac{e\psi(z)}{k_{\mathrm{B}}T}\right) - \exp\left(\frac{e\psi(z)}{k_{\mathrm{B}}T}\right)\right\}, \tag{2}$$

where e, n_0, k_{B} and T are the magnitude of electron charge, bulk density of electrolyte in equilibrium with the electrolytes within the channel, the Boltzmann constant, and the temperature, respectively.

In the theory of Levine *et al.* [5], the z-dependent velocity profile is determined by solving the Navier–Stokes equation in one-dimension with the no-slip boundary condition

$$\eta\frac{\mathrm{d}^2u(z)}{\mathrm{d}z^2} = -\rho(z)E,\ u(0) = u(d) = 0, \left.\frac{\mathrm{d}u(z)}{\mathrm{d}z}\right|_{d/2} = 0, \tag{3}$$

where $u(z)$ is the fluid flow velocity and E is the applied electric field, both in the direction parallel to the plates, and η is the viscosity of the fluid. It is also assumed that there are no slip at the walls and no velocity gradient at the midplane in the channel.

Based on Eqs. (1) and (3), the velocity, $u(z)$, and the electrostatic potential are related to each other by

$$u(z) = \frac{\varepsilon E}{4\pi\eta}(\psi(z) - \zeta). \tag{4}$$

Averaging across the channel gives the average velocity for the electroosmotic flow

$$\langle u(z)\rangle = \frac{\varepsilon E}{4\pi\eta}(\langle\psi(z)\rangle - \zeta), \tag{5}$$

where averages are denoted by the angular brackets.

Equations (1) and (3) suggest that if the electric charge density distribution can be determined, the integration of the electric charge density can be carried out to determine the electric potential and the velocity profile across the channel. In this work, the electric charge density profile is determined from molecular simulation, without the assumption of the Boltzmann distribution for the ions near the wall, which becomes unreliable at high ζ-potential.

Molecular dynamics simulations have been carried out for monovalent electrolyte solutions in parallel-plate channels to study the electroosmotic flow of the fluid. In the simulation, the solvent is treated as a dielectric continuum with a dielectric constant, $\varepsilon = 59.24$, and viscosity $\eta = 1.68$ cP. This corresponds to a solvent mixture of methanol and water. The reason such a system is chosen instead of water as the solvent is that nanofluidic experiments have recently been performed using such solvent [6]. This allows us to verify the predictions from

TABLE I Debye length and the ζ-potential for the fluid studied [6]

Concentration (*mM*)	$1/\kappa$ (*nm*)	ζ (*mV*)
0.2	18.86	138
2	5.96	98
20	1.89	54

the theory and the simulation. The conclusions drawn from the simulation results are of course general with ε and η as the material parameters. The Debye length, $1/\kappa$, and the electrostatic potential at the walls, i.e. the ζ-potential, are tabulated in Table I [6]. The monovalent positive and negative ions were chosen to be Na^+ and Cl^-. The ions interact with each other through the Coulomb electrostatic potential and Lennard–Jones potential. The parameters of the Lennard–Jones potentials are listed in Table II. In our simulations, the Lennard–Jones interactions were truncated at a cutoff distance of 11.08 Å. The wall-fluid interaction is described by a purely repulsive potential

$$V(z) = 4\varepsilon_0\left(\frac{\sigma}{z - z_0}\right)^{10}, \qquad (6)$$

where $\varepsilon_0 = 0.6502\,\text{kJ/mol}$, and $\sigma = 3.166\,\text{Å}$. For simplicity we used the same potential for the interactions between the wall and both positive and negative ions. z_0 is the position of the wall, and z is the position of an ion in the fluid. Since the channel widths in this study are generally very large compared to the size of solvent molecules and ions, we have neglected the fine details of the structure near the wall, which would become relatively more important for small channels of widths 5 nm and less.

The electric charges on the walls were described by a continuous distribution. The total electric charges on the opposite walls are neutralized by the excess counter-ions in the solution. According to electrostatics, a uniform charge distribution on an infinite plate results in an electric field, $\vec{E} = \pm 2\pi\sigma_e\hat{z}/\varepsilon$ [8], where σ_e is the surface charge density, $\hat{z}$ is the unit vector normal to the walls, and ε is the dielectric constant, as defined before. The $\pm$ signs correspond to the two walls with normal in the positive and negative z-direction. Since $\vec{E}$ does not depend on the position of charges in the fluid, the net electric force by the two walls on a charge in the fluid is zero. Here for simplicity, we have assumed the fluid and the walls have the same dielectric constant, so that the image charge effect can be neglected. For the parallel-plate systems considered here, the fluid is confined in z-direction only and infinite in the other two directions. So periodic boundary conditions are used in the two unbounded directions. To treat the long-range Coulomb interaction, the Ewald summation method appropriate to the two-dimensional fluid has to be used. There are a number of approaches for 2D Ewald summation methods [9]. We have chosen the method by Hayes *et al.* [10] for its accuracy, although it is computationally more expensive.

TABLE II The Lennard–Jones interaction parameters for the sodium and the chloride ions

Pair	σ (*Å*)	$\varepsilon(kJ\,mol^{-1})$
Na^+–Na^+	2.73	0.3576
Cl^-–Cl^-	4.86	0.1679
Na^+–Cl^-	3.87	0.1706

The equations of motion were integrated using the Verlet method [11]. The temperature of the system was kept at 300 K using the Berendsen thermostat [12]. For all the simulations reported here, the surface charge density was kept constant for a given ion concentration as the channel width varied. The concentration of the co-ions, Cl^- in our case, depends slightly on the channel width only when the width of the electric double-layer become significant relative to the channel width, about 10 nm. To be consistent with the theory of Levine *et al.*, the co-ion concentrations were determined using the theory. The correctness of the approach is justified by the simulation results (see Fig. 4 below) where the co-ion distributions obtained from the simulation and the theory are found to be essentially identical.

RESULTS AND DISCUSSION

Ion Distribution and Velocity Profile for Channel Widths at 120 nm with Varying Ionic Concentration

Figure 1(a) and (b) shows the ion density distributions obtained from molecular simulation for the channel width of 120 nm at concentration $n_0 = 2$ and 20 mM. As seen in Fig. 1(a), in a large region away from the wall, the concentrations of positive and negative ions are equal. For $n_0 = 20\,\text{mM}$, the extent of the non-neutral region is about 10 nm. For $n_0 = 2\,\text{mM}$, the extent of the non-neutral region is about 20 nm.

The ion density distributions in Fig. 1(a) lead to electric charge density distribution, $\rho(z) = e[n^+(z) - n^-(z)]$., where $n^+(z)$ and $n^-(z)$ denote the number density of the positive and negative ions. Integrating Eq. (3), we obtained the velocity of the fluid, normalized by the parameters characterizing the fluid, η and ε, and the applied electric field, E. In Fig. 1(b), we present the non-dimensionalized velocity, $V/(eE/\eta)$, which apart

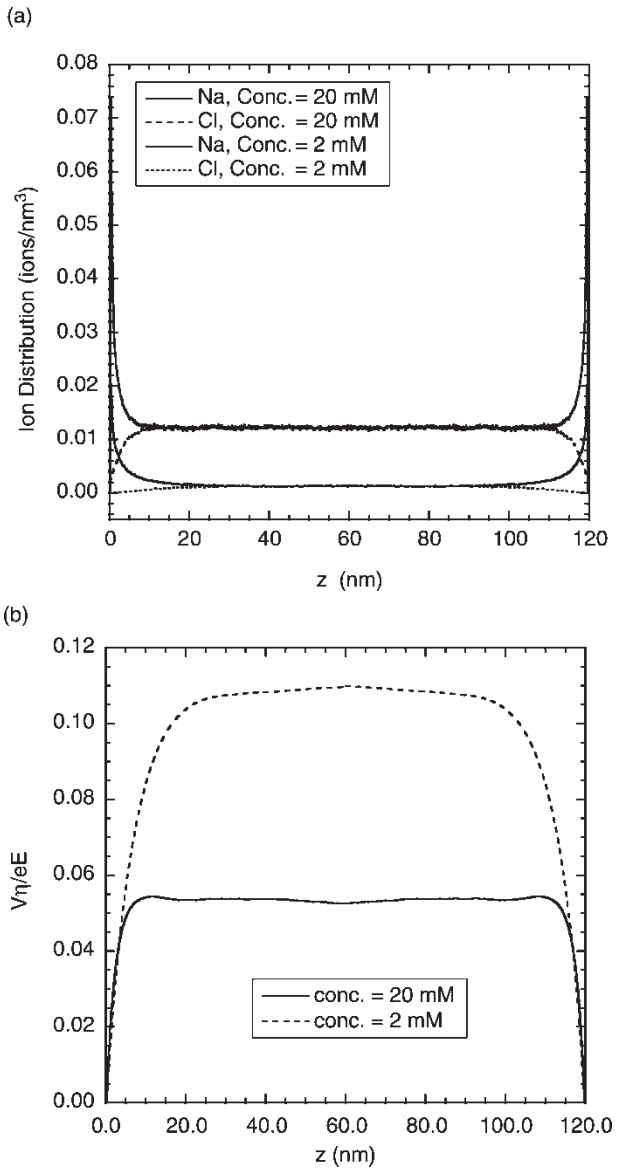

FIGURE 1 (a) Ion distributions for the 120 nm channel at ion concentrations 2 mM (the two lower curves) and 20 mM (the two upper cuves). Solid curves are for the counter-ions (Na^+) and the dashed curves are for the co-ions (Cl^-). (b) The reduced velocity profiles corresponding to (a). Solid curve: ion concentration at 20 mM; dashed curve: ion concentration at 2 mM.

from a proportionality constant, also represents the position dependent mobility $\langle u(z)\rangle/E$. It is seen from Fig. 1(b) that the velocity profiles for both $n_0 = 2$ and 20 mM have an extended constant-velocity, plug flow region. The constant-velocity region corresponds to the electrically neutral region in the charge distribution. It is also notable that the constant velocity is higher for the lower concentration, 2 mM, than for the higher concentration, 20 mM. This is related to the experimental fact that for channels made of silica, the ζ-potential is higher at lower concentration, as can be seen from Table I.

Ion Distribution and Velocity Profile for Varying Channel Width at Ionic Concentration of 20 mM

To further study the effect of electrical double-layer overlap, we plot in Fig. 2(a) the ion distributions at $n_0 = 20$ mM as the channel width narrows. In the figure, we have normalized the z-position by the width of the channel so that results for different channel width can be compared in the same figure. It is seen from Fig. 2(a) that as the channel width narrows from 40 to 10 nm, the positive and negative ion distributions in the middle region of the channel become increasingly more separated. For the 40 nm channel, there is a charge neutral region where the positive and negative ion distributions are equal. For channel width 20 nm, the positive and negative ion distributions begin to separate slightly in the entire channel. For the 10 nm channel, the separation of the density distributions becomes large. Figure 2(b) shows the velocity profiles for the fluid flow corresponding to the ion distributions in Fig. 2(a). It is seen that the velocity profiles exhibit a shape that becomes increasingly curved at the center of the profile as the channel width decreases. We used polynomials to fit the flow profiles. It is found that for the 10 nm channel, the flow profile can be fitted by a parabolic form. For the 20 nm channel, a fourth order polynomial has to be used to fit the flow profile. For the 40 nm channel, an eighth order polynomial is needed to describe the flow. These results show the transition to parabolic flow is gradual, rather than an abrupt transition from plug flow to parabolic flow. It is also noted that at a fixed concentration, the peak velocity becomes lower as the channel width decreases.

Comparison of Ion Distribution and Velocity Profile for 2 and 20 mM Ionic Concentration

In Fig. 3(a) and (b), we show the ion distribution and velocity profile for channel width at 40 nm and concentrations at 2 and 20 mM. This can be compared with the result for channel width at 120 nm in Fig. 1. For $n_0 = 20$ mM, the density distribution still shows a region where the positive and negative ions have the same density, implying an electrically neutral region. Note the Debye length is 1.89 nm, much smaller than the channel width. For $n_0 = 2$ mM, we see that the density distributions for the positive and negative charges become separated in the entire channel. It is worth noting that at 2 mM ionic concentration, the half channel width, 20 nm, is still significantly larger than the Debye length, 5.96 nm (see Table I). The onset of the effect of double-layer overlap may begin at

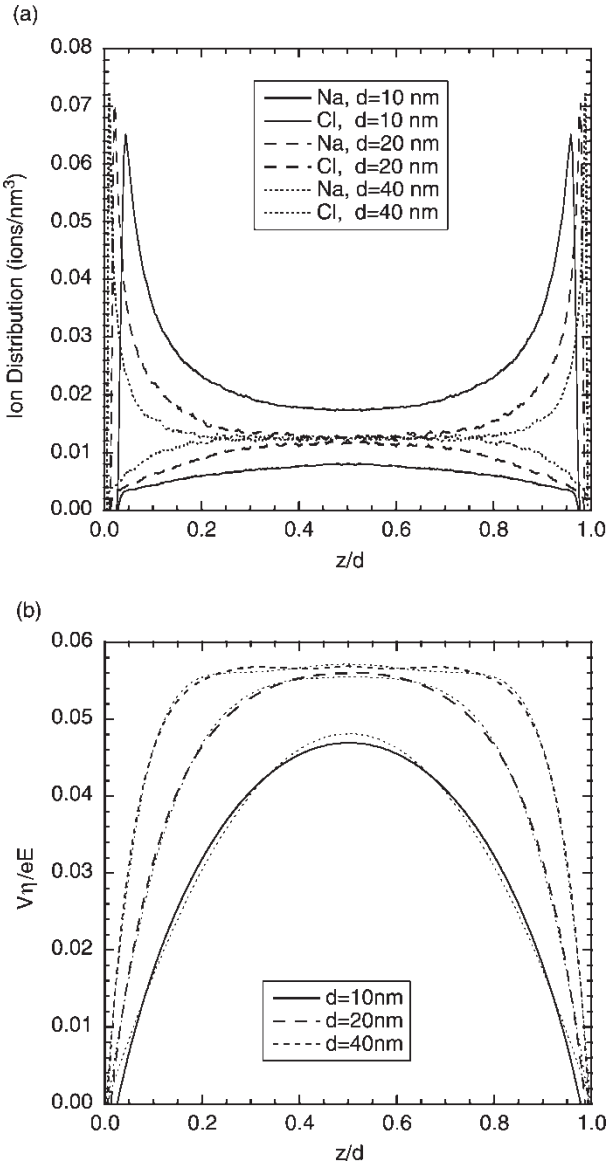

FIGURE 2 (a) Ion distributions for varying channel width from 10 to 40 nm at ion concentration 20 mM. Solid curve: 10 nm channel; long-dashed curves: 20 nm channel; short-dashed curves: 40 nm channel. (b) The reduced velocity profiles corresponding to (a). The solid, long-dashed, and short-dashed curves are for 10, 20, and 40 nm channels, respectively.

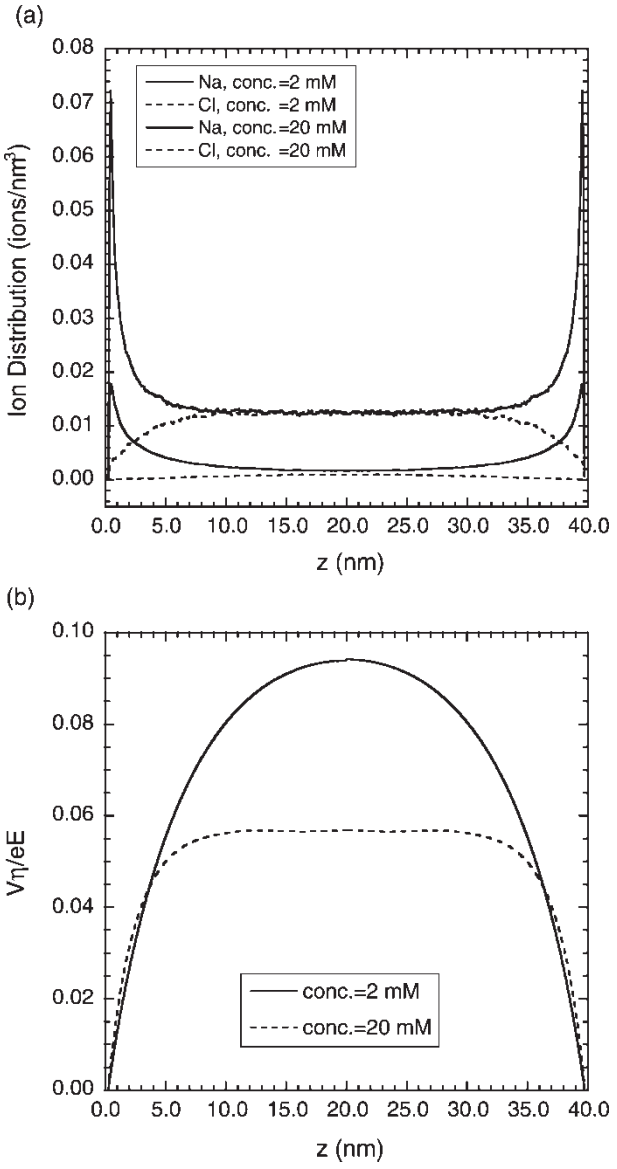

FIGURE 3 (a) Ion distributions for the 40 nm channel showing the effect of electrical double-layer overlap. The upper curves are for concentration 20 mM and the lower curves are for the concentration of 2 mM. The solid curves are for the counter-ions (Na^+) and the dashed curves are for the co-ions (Cl^-). (b) The velocity profiles showing the plug flow at concentration 20 mM (dashed curve) and the parabolic flow at concentration 2 mM (solid curve) corresponding to the ion distributions in (a).

a channel width significantly larger than the Debye length because the slowly varying tail of the ion distribution has a much larger range than the exponential decrease characterized by the Debye length. The velocity profiles for $n_0 = 2$ and 20 mM are shown in Fig. 3(b). As expected, the velocity profile for $n_0 = 20$ mM shows a significant region of plug flow, but there is a significant boundary effect. For $n_0 = 2$ mM, the velocity profile shows clearly a parabolic type velocity profile, as a result of the overlap of the electric double-layer. Again, the peak of the velocity for the lower concentration is higher than the peak velocity for the higher concentration.

Comparison between the Simulation and the Theory

Figure 4(a) shows the comparison of the ion density distributions for the 120 nm channel at 20 mM between the molecular simulation and the classical Poisson–Boltzmann theory by Levine *et al.* For clarity we plot only the part of the curves within 20 nm of the wall. It is seen that at 20 mM concentration, the simulation and the theory have very good agreement. The co-ion (negative ion) distributions are essentially identical. For the counter-ions (positive ions), except for some minor difference at

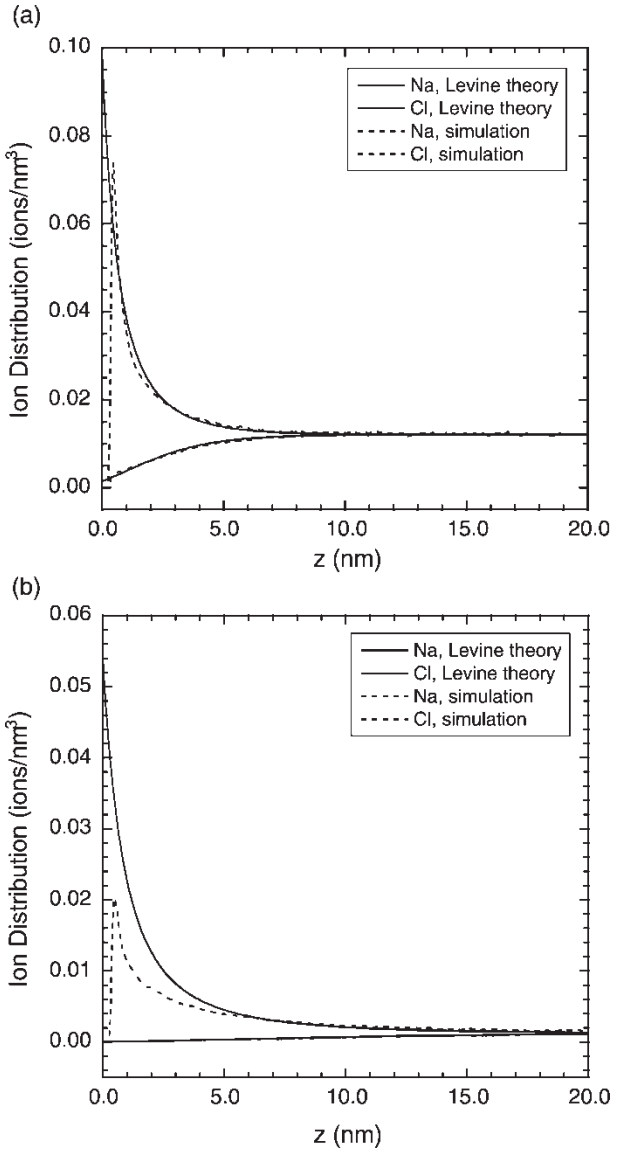

FIGURE 4 (a) Comparison of the ion distributions for the 120 nm channel at ion concentration 20 mM between the Levine theory and simulation. Solid curves: theory; dashed curves: simulation. (b) The same as in (a), but for ion concentration 2 mM.

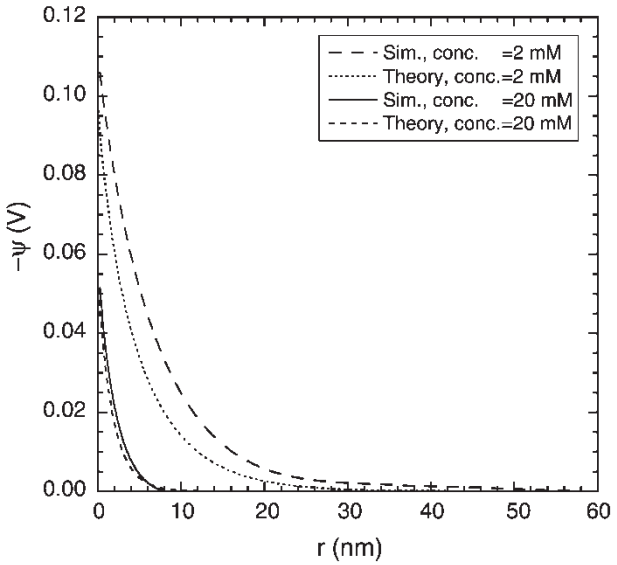

FIGURE 5 The electrostatic potentials obtained from the theory and simulation. Solid and short-dashed curves: simulation and theory, respectively, at concentration 20 mM. Long-dashed and dotted curves: simulation and theory, respectively, at concentration 2 mM.

the wall (the excluded volume effect in the simulation prevents the ions from accessing the space within about 2–3 Å to the wall), the density distributions also agree very well between the theory and the simulation. We note that the ζ-potential at 20 mM is 54 mV, for which the exponent in the Boltzmann distribution is about 2 at room temperature. This is near the boundary where the Poisson–Boltzmann theory is commonly believed to start to break down.

Figure 4(b) shows the same comparison between the theory and simulation at 2 mM ionic concentration. We see that the co-ion distributions from the theory and the simulation are again identical. For the counter-ions, however, the theory significantly overestimates the ion density near the wall while at large distance from the wall, the difference is very slight. The ζ-potential for the 2 mM concentration is 98 mV, giving an exponent about 4 at room temperature in the Boltzmann distribution. This leads to a very large exponential factor for the counter-ions in the Boltzmann distribution. The results presented here thus demonstrate that the classical Poisson–Boltzmann equation, even with the full Boltzmann distribution, becomes inaccurate for determining the counter-ion density distribution at ζ-potential significantly larger than about 50 mV. It is well-known in literature that the Boltzmann distribution does not take into account the inter-ionic correlation [13]. This effect is apparently exacerbated at high surface potential.

In Fig. 5, we show the electrostatic potential for the channel width of 120 nm at two concentrations, 2 and 20 mM. It is seen that at 20 mM concentration, the electrostatic potential from the theory and the simulation almost overlap. At 2 mM concentration, the electrostatic potential from the simulation is higher by about 6 mV than the theoretical prediction. It appears that despite the inaccuracy for the counter-ion distribution in the Boltzmann distribution at high ζ-potential, the theory gives better prediction for the electrostatic potential, as it does not directly use the charge density but directly solves for the electrostatic potential.

We make clear that the theoretical analysis in this paper used a fixed constant electrostatic potential at the boundary. For simplicity in simulation we have used constant charge density at the boundary. The difference in the counter-ion distribution

between the theory and the simulation, however, was not the result of the different boundary conditions used. At 20 mM ionic concentration ($\zeta = 54$ mV), the theory and the simulation give very good agreement for both the ion density distribution (Fig. 4) and the electrostatic potential (Fig. 5). At 2.0 mM ionic concentration ($\zeta = 98$ mV), however, the counter-ion density distribution from the theory is significantly larger than from the simulation, while the co-ion density distributions are the same. This implies a higher surface charge density in the theory to satisfy total charge neutrality. Thus, to compensate the difference, we would need a higher charge density than that used in the simulation. But as shown in Fig. 5, the electrostatic potential from simulation is actually higher than that from the theory. To bring the electrostatic potential to the same value as in theory would require decreasing the surface charge density used in the simulation, further exacerbating the difference of the counter-ion density distributions between theory and simulation. The basic reason for the difference between theory and simulations is the assumption of the Boltzmann distribution in the theory. Its exponential increase for counter-ions seems too strong to be realistic at high surface potential. Many authors have pointed out its inconsistency with the linear superposition principle of the electrostatic interaction [14,15,17]. The issue has been discussed in literature [14–17]. It appears that the Boltzmann distribution for the counter-ions does not take into account the non-linear effect in an appropriate manner at high electrostatic potential. Inherent in the Boltzmann distribution is the neglect of inter-ionic correlation and the excluded volume effect, although the Poisson equation is fundamentally correct. Use of a modified Boltzmann distribution function has thus been proposed in literature [18–20].

Mobility from Theory and Simulation

Figure 6 shows the average mobility obtained from the theory and the simulation, defined as $\langle u(z)\rangle/E$, the average fluid velocity divided by the applied electric field E. We first point out that we have chosen the surface charge density such that at large channel width, the mobility obtained from simulation agrees with recent experiments of Alarie *et al.* [6]. Comparison of the theory and the simulation shows that, at 20 mM, the average mobility obtained from theory and simulation agrees very well in the range covered by simulation, ~10–120 nm. At lower concentration, 2 mM, the mobility obtained from the theory tends to be slightly lower than from simulation at large channel width. As the channel width decreases, the mobility decreases, and the mobility obtained from simulation tends to decrease more rapidly than that from the theory. At very low concentration, 0.2 mM, the theory predicts a mobility lower than simulation at large channel width, while at channel width less than about 100 nm, the mobility from simulation again shows a trend of more rapid decrease. We note, however, that had we adjusted the surface charge density to produce a mobility that agrees with the theory at large channel width, the simulation would have given a mobility that is too low at small channel width.

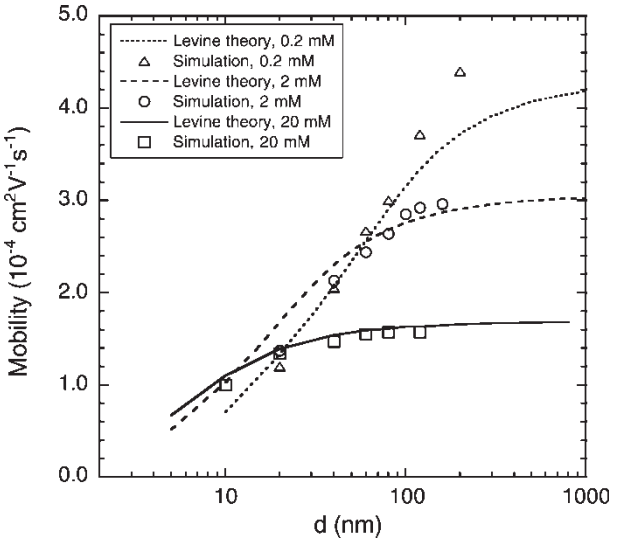

FIGURE 6 Electroosmotic flow mobility obtained from theory and simulation. Symbols are from simulation and the curves are from the theory. Squares and solid curve: 20 mM concentration; circles and long-dashed curves: 2 mM concentration; triangles and short-dashed curves: 0.2 mM concentration.

Overall, the theory of electroosmotic flow quite reasonably captures the general trend of the mobility variation with the channel width in the range about 10 to 100 nm. The higher counter-ion density near the wall, resulting from the assumption of the Boltzmann distribution for the ions, clearly contributes to a higher mobility for the narrow channel width less than about 100 nm. This becomes increasingly more significant as the channel narrows.

CONCLUSIONS

In this work, we have carried out molecular dynamics simulation using the continuum solvent model to study electroosmotic flow in parallel-plate channels for channel width in the range about 10 to 120 nm at low to moderate ion concentrations commonly used in fluidic device operation. Using the results obtained from the molecular simulation, we examined the applicability of the classical theory based on the Poisson–Boltzmann equation with the full Boltzmann distribution for the ions without linearization. We found that the classical

theory can reasonably predict the fluid mobility of electroosmotic flow for moderate ion concentrations around 20 mM. At low ion concentration, the classical theory appears to predict a more rapid decrease of the fluid mobility as the channel width decreases, while capturing the qualitative trend of the mobility variation as the channel width narrows from 100 to about 10 nm. Although the present work considered essentially model silica channels through the characterization of the ζ-potential appropriate for silica channels, the general conclusion is that the classical theory becomes inaccurate when the ζ-potential significantly exceeds about 50 mV. This is the case even when the full Boltzmann distribution is used for the ion distributions.

Acknowledgements

The authors acknowledge many helpful discussions with Mike Ramsey and his group. This work is supported in part by the NSF at UT under contract BES-0103140, by DARPA at ORNL, and by the Chemical Sciences Division of DOE at ORNL. ORNL is operated for the U.S. DOE by UT-Battelle, LLC, under contract DE-AC05-00OR22725.

References

[1] Schasfoort, R.B.M., Schlautmann, S., Hendrikse, J. and van den Berg, A. (1999) "Field-effect flow control for microfabricated fluidic networks", *Science* **286**, 942.
[2] Fister, J.C., III, Jacobson, S.C., Davis, L.M. and Ramsey, J.M. (1998) "Counting single chromophore molecules for ultrasensitive analysis and separations on microchip devices", *Anal. Chem.* **70**, 431.
[3] Weigl, B.H. and Yager, P. (1999) "Microfluidic diffusion-based separation and detection", *Science* **283**, 346.
[4] Jorgenson, J.W. and Lukacs, K.D. (1981) "Zone electrophoresis in open tubular glass capillaries", *Anal. Chem.* **53**, 1298.
[5] Levine, S., Marriott, J.R. and Robinson, K. (1975) "Theory of electrokinetic flow in a narrow parallel-plate channel", *J. Chem. Soc. Faraday Trans. 2*, **71**, 1.
[6] Alarie, J.P., Jacobson, S.C., Peterson, N.J., Cui, S.T. and Ramsey, J.M. (2003) "Nanofluidics: Molecular Transport through Nanometer Deep Channels", to be submitted.
[7] Debye, P. and Hückel, E. (1923) "Zur Theorie der Elektrolyte. I. Gefrierpunktser-niedrigung und verwandte Erscheinungen", *Z. Phys.* **24**, 185.
[8] Jackson, J.D. (1975) *Classical Electrodynamics*, 2nd Ed. (John Wiley & Sons, Inc., New York).
[9] Widmann, A.H. and Adolf, D.B. (1997) "A comparison of Ewali summation techniques for planar surfaces", *Comp. Phys. Comm.* **107**, 167.
[10] Heyes, D.M., Barber, M. and Clarke, J.H.R. (1977) "Molecular dynamics computer simulation of surface properties of crystalline potassium chloride", *J. Chem. Soc. Faraday Trans. 2* **73**, 1485.
[11] Allen, M.P. and Tildesley, D.J. (1987) *Computer Simulation of Liquids* (Oxford University Press, Oxford).
[12] Berendsen, H.J.C., Postma, J.P.M., van Gunsteren, W.F., Dinola, A. and Haak, J.R. (1984) "Molecular dynamics with coupling to an external bath", *J. Chem. Phys.* **81**, 3684.
[13] Hribar, B., Vlachy, V., Bhuiyan, L.B. and Outhwaite, C.W. (2000) "Ion distribution in cylindrical capillary as seen by the modified Poisson-Boltzmann theory and Monte-Carlo simulations", *J. Phys. Chem. B* **104**, 11522.
[14] Bockris, J.O. and Reddy, A.K. (1998) *Modern Electrochemistry: Ionics*, 2nd Ed. (Plenum Press, New York) Vol. **1**.
[15] Onsager, L. (1933) "Theories of concentrated electrolytes", *Chem. Rev.* **13**, 73.
[16] Lampert, M. (1985) "The non-linear poisson-Boltzmann equation", *Nature* **315**, 159.
[17] Spitzer, J.J. (1984) "A re-interpretation of hydration forces near charged surfaces", *Nature* **310**, 396.
[18] Carnie, S.L. and Torrie, G.M. (1984) "The statistical mechanics of the electrical double layer", *Adv. Chem. Phys.* **56**, 141.
[19] Outhwaite, C.W. (1986) "A modified Poisson-Boltzmann equation for the ionic atmosphere around a cylindrical wall", *J. Chem. Soc. Faraday Trans. 2*, **82**, 789.
[20] Bhuiyan, L.B. and Outhwaite, W. (1994) "The cylindrical electric double layer in the modified Poisson-Boltzmann theory", *Philos. Mag. B* **69**, 1051.